*Geologica Acta, Vol.11, Nº 3, september 2013, 265-276*
**DOI: 10.1344/105.000001870**
*Available online at www.geologica-acta.com*

**geologica acta**

# Multidetachment analogue models of fold reactivation in transpression: The NW Persian Gulf

**B. SOLEIMANY** [1] **T. NALPAS** [2] **F. SÀBAT** [3,*]

[1] **National Iranian Oil Company, Exploration Directorate**
Seoul Ave.,Tehran,1994814695, Iran

[2] **Géosciences Rennes, UMR 6118 du CNRS, Université de Rennes 1**
Campus de Beaulieu, 35042 Rennes cedex, France

[3] **Departament de Geodinàmica i Geofísica, Facultat de Geologia, Universitat de Barcelona**
C/ Martí i Franqués, s/n, 08028, Spain. Sàbat E-mail: sabat@ub.edu

*Corresponding author

## ABSTRACT

Two deformation events have been documented in the NW Persian Gulf that occurred during the Late Cretaceous and the Late Cenozoic. The most distinctive feature in this part of the Persian Gulf is the reactivation of the Late Cretaceous NNE-SSW Arabian trending folds by NE-SW shortening during the Late Cenozoic Zagros Orogeny. In general, if a set of folds with horizontal axes is shortened roughly parallel to its fold axis, a dome-basin fold interference pattern is produced. In the NW Persian Gulf, reactivation of some old folds occurred instead of a fold interference pattern. Reactivation may be influenced by the following factors: i) the presence of incompetent layers (*i.e.* evaporites), ii) a variable overburden, iii) basement faults, and iv) obliquity between the younger deformation shortening axis and fold axis. It is this last factor that we investigated by means of analogue modelling. The experimental apparatus is similar to that commonly used for experiments with brittle-ductile systems at the Laboratory of Experimental Tectonics of Géosciences Rennes. The model consisted of an alternation of ductile and brittle horizontal layers with a stratigraphy similar to the one found in the NW Persian Gulf. The model was deformed by two deformation events with an angle $\alpha$ between the two directions of shortening. After deformation, the resulting structure resembled a fold facing the static wall with internal thrust faults and detachment faults arranged into a geometry similar to a fish tail. In the second shortening event, the fold was reactivated without formation of an interference pattern. Moreover, the displacement on both the reactivated and newly formed faults varied between almost pure thrust faults for low $\alpha$ and oblique thrust faults with a strike-slip component for high $\alpha$. The models suggest that the presence of incompetent layers plays an important role in fold reactivation and confirm that basement faults are not necessary.

***KEYWORDS*** | **Analogue modelling. Reactivation. Multi detachment. Compression. Transpression. Persian Gulf.**

## INTRODUCTION

The NW Persian Gulf provides good examples of folds reactivated by a later longitudinal compression. These folds involve a stratigraphic sequence that consists of a multilayer with alternating ductile and brittle layers (O'Brien, 1950; Sepehr *et al.*, 2006; Casciello *et al.*, 2009). The stratigraphic pile and the set of structures resulting from the first deformational event exert a strong influence on the way that these structures behave when undergoing further deformation.

Pre-existing faults are zones of weakness that influence the organization and evolution of deformation in sedimentary basins. Reactivation of pre-existing structures has been extensively studied in nature (*e.g.* Harding, 1985; Mescua and Giambiagi, 2012), in theoretical analysis (*e.g.* Sibson, 1985; Letouzey, 1990) and in analogue modelling (*e.g.* Koopman *et al.*, 1987; Richard and Krantz, 1991). Earlier studies using analogue modelling in a compressive or transpressive setting have highlighted the role of sedimentation in the resulting structures for models with one detachment level (Casas *et al.*, 2001; Barrier *et al.*, 2002; Nalpas *et al.*, 2003) or two detachment levels (Gestain *et al.*, 2004; Pichot and Nalpas, 2009; Emami *et al.*, 2010). Analogue modelling studies related to reactivation of a previous fault have underlined: i) the role of oblique compression during basin inversion (Nalpas *et al.*, 1995; Brun and Nalpas, 1996); ii) the type of strike-slip structures created during the oblique reactivation of a previous high dipping fault (Richard *et al.*, 1989; Richard and Cobbold, 1990; Richard *et al.*, 1991); iii) the role of pre-existing faults in thrust tectonics (Sassi *et al.*, 1993); and iv) the effect of the location and orientation of pre-existing faults related to the new stress field (Richard and Cobbold, 1990; Faccenna *et al.*, 1995; Dubois *et al.*, 2002). However, there have been no experiments on the reactivation of previous compressive structures in a second shortening event for models in which the shortening direction is variable and in which there are different detachment levels.

The aim of this paper is to study the reactivation of pure compressive structures during a second event of compression characterized by an oblique direction of shortening with respect to the first set of structures. To this end, we used analogue models in which the deformed stratigraphic package included several ductile detachment levels. Some geological features of the NW Persian Gulf will be reviewed before analogue modelling in order to allow comparison between the results of the model and the structures in this area.

Transpression is a strike-slip deformation that deviate from simple shear because of a component of shortening orthogonal to the deformation zone (Dewey *et al.*, 1998).

## GEOLOGY OF THE NW PERSIAN GULF

Regional geology of the Persian Gulf has been described and analysed in detail because of the high hydrocarbon potential of this region (Stern, 1985; Alsharhan and Nair, 1997; Beydoun, 1991; Edgell, 1996; Bahroudi and Talbot, 2003). Soleimany and Sàbat (2010) describe the stratigraphy and fold structures in the NW Persian Gulf (Fig. 1A) using data from seven wells and 2760km of seismic profiles. A simplified mechanical stratigraphy column of this area displays the superposition of three alternating ductile and three brittle layers (Fig. 1B). The uppermost brittle layer consists of upper Miocene - Pliocene marine sandstone and siltstone. The upper part of the layer is coeval with the main deformation stage of the Zagros Orogeny (*e.g.* Homke *et al.*, 2004). The upper ductile layer is composed of Miocene gypsum, anhydrite, salt, marls and dolomite. The Eocene and Oligocene brittle layer is made up of limestones and dolomitic limestones. The Upper Cretaceous growth strata consist of marine shales, marls and limestones. The Jurassic and Cretaceous brittle layer is mainly constituted by limestones and dolomites, but shales, sandstones and anhydrite are also present. The Triassic ductile layer is made up of gypsum and anhydrite interbedded with dolomites and limestones. The Paleozoic brittle layer is composed of shales, silstones, sandstones and conglomerates and includes Cambrian and Permian limestones and dolomites. The lower ductile layer consists of Cambrian salt and anhydrite.

According to Soleimany and Sàbat (2010), the NW Persian Gulf folds resulted from two deformation events which occurred at the end of the Late Cretaceous and in the late Cenozoic. The age of these deformation events is clearly demonstrated by the growth strata visible in seismic sections (Fig. 1C). Folds in this area show different styles, from symmetric to westward vergent, and are not regularly distributed along the section. No major thrust, detachment or basement faults are visible in the seismic sections (*e.g.* Fig. 1C).

In the late Cretaceous deformation event (James and Wynd, 1965; Saura *et al.*, 2011), a number of NNE-SSW trending folds (termed "Arabian trend" hereinafter) were formed (Fig. 1D, A1 and A8 folds) and a strong Maastrichtian unconformity is visible in the seismic sections all around the area (*e.g.* Fig. 1C).

The late Cenozoic deformation event corresponds to the Zagros Orogeny. The Zagros Range consists of a NW-SE striking fold and thrust belt resulting from NE-SW shortening (Stöcklin, 1968; Alavi, 1994) due to N-S convergence (Sella *et al.*, 2002) between the Arabian Plate and the Iranian Block (Eurasian Plate).

In the NW Persian Gulf, folding was complicated by the simultaneous growth of folds with different trends during the younger deformation event (Soleimany and Sàbat, 2010). These trends, which can be observed in the contour map of the late Miocene horizon (Fig. 1E), are as follows:

i) The NNE-SSW (*i.e.* A1 M) to N-S (*i.e.* A3 M) trend. This trend is well represented in the northern part of the map. Folds with this trend result from the reactivation of the deep seated Arabian trending folds of Late Cretaceous age.

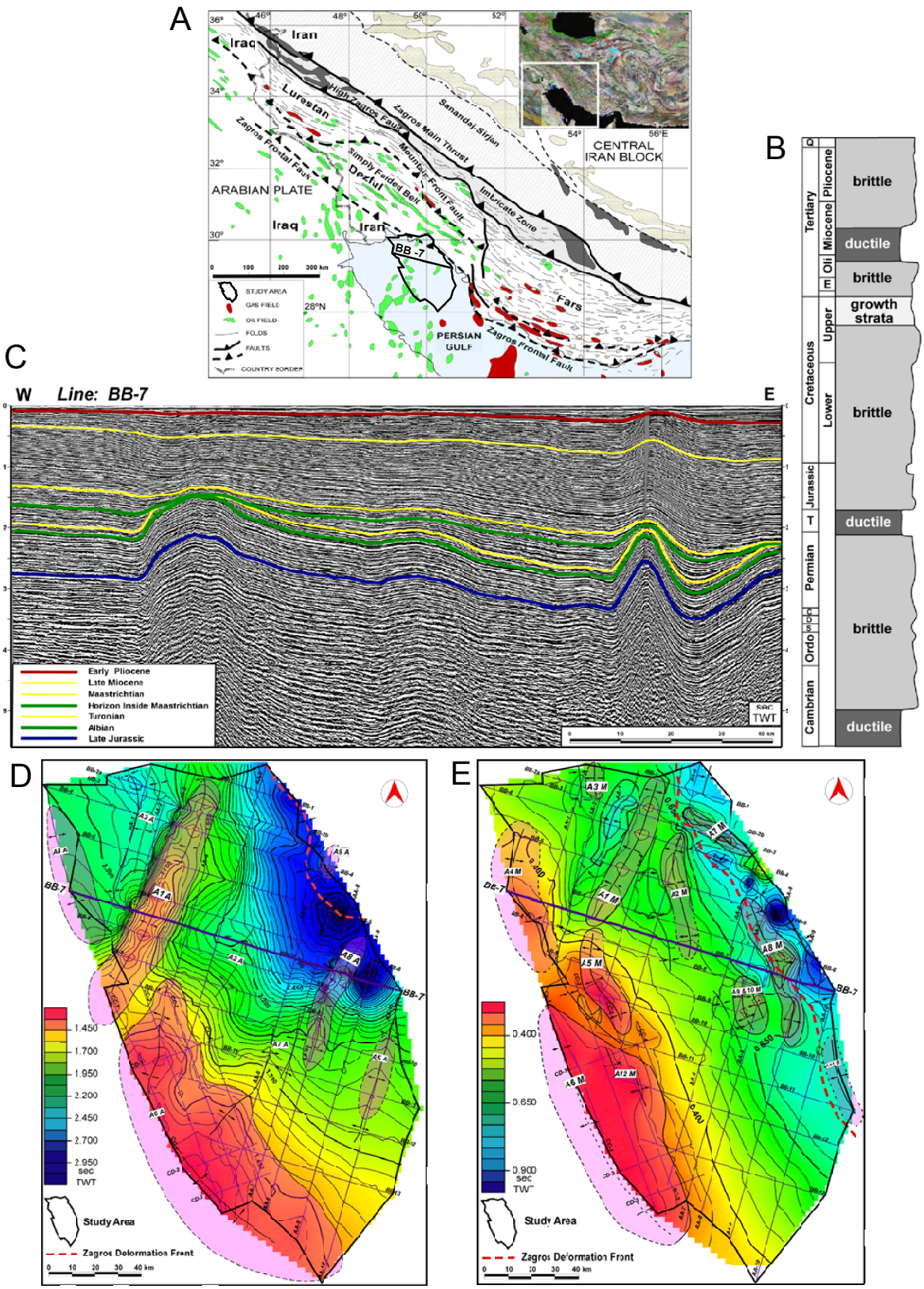


**FIGURE 1** | A) Location of the study area in the Persian Gulf in the foreland of the Zagros Range. Modified from Vergés *et al.* (2009). B) Mechanical stratigraphy of the study area. C) Seismic section BB-7 (see location in A, D, E). Modified from Soleimany and Sàbat (2009). D) contour map of the top of the Albian Kazhdumi Formation in the study area. E) Contour map of the top of the late Miocene Mishan Formation in the study area.

**TABLE 1** | Scaling parameters. L: length; g: gravity; ρρ: density; μ: viscosity; V: velocity; t: time; ρσ: stress

| | L (m) | g ($m/s^2$) | ρ ($Kg/m^3$) | μ (Pa.s) | V (m/s) | t (s) | σ (Pa) |
|---|---|---|---|---|---|---|---|
| Nature | 1000 | 9.81 | 2300 | $2 \times 10^{18}$ | $1.6 \times 10^{-10}$ (0.5 cm/y) | $3.2 \times 10^{13}$ (1 Ma) | $2.3 \times 10^{6}$ |
| Model | 0.01 | 9.81 | 1400 | $3.5 \times 10^{4}$ | $5.6 \times 10^{-6}$ (2 cm/y) | $9.2 \times 10^{3}$ (2.5 h) | 14 |
| Model/Nature Ratio | $10^{-5}$ | 1 | 0.6 | $1.8 \times 10^{-15}$ | $3.5 \times 10^{4}$ | $2.9 \times 10^{-10}$ | $6 \times 10^{-6}$ |

ii) The NW-SE trend (*i.e.* A7 M). This trend is only present in the northeastern part of the map. Folds with this trend correspond to the NW-SE Zagros folds and are due to NE-SW shortening.

iii) The NNW-SSE trend. This is S-shaped in surface view (*i.e.* A5 M, A8 M, etc.). Folds with this shape seem to be due to the interaction between the Zagros and Arabian folds given that one part of the fold trends NNE-SSW whereas the other part trends NW-SE.

iv) The NNW-SSE trend. A huge anticline is present in the southwestern part of the map (A6 M) and is also observed in the contour map of the Albian horizon (Fig. 1D). This anticline could be part of the peripheral bulge related to the foreland flexure induced by the load of the Zagros Range.

The most distinctive feature in this part of the Persian Gulf is that the late Cenozoic NE-SW shortening reactivated the Late Cretaceous NNE-SSW Arabian trending folds (Soleimany and Sàbat, 2010). This feature is supported by two arguments: i) in the E-W seismic sections (*e.g.* Fig. 1C), the Mesozoic horizons, the Late Cretaceous unconformity and the Cenozoic horizons are affected by the Arabian trending folds but the folds below the unconformity are more tightly folded than the ones above the unconformity (this is clearly observed in the anticline in the eastern part of seismic section BB-7, Fig. 1C); ii) the Arabian folds grew during Late Cretaceous as evidenced by the Late Cretaceous growth strata imaged in seismic sections (*e.g.* Fig. 1C). Moreover, the contour maps of Cenozoic horizons (Fig. 1E) show that these horizons are also folded by the Arabian trending folds. In surface view, the Cenozoic Arabian folds are spatially related to the Late Cretaceous Arabian folds (compare Fig. 1D and E, A1, A6 and A8 folds).

In general, if a set of folds with horizontal axis is shortened roughly parallel to its fold axis, a dome-basin fold interference pattern is produced (fold interference type 1 of Ramsay and Huber, 1987). However, in the NW Persian Gulf, the reactivation of some old folds occurred instead of the aforementioned fold interference pattern. Reactivation of old folds during younger deformation events could be due to a number of factors: i) the presence of a regional mechanical anisotropy due to a variable overburden on the older folds and/or to the competent-incompetent alternation folded by older folds, ii) the reactivation of basement faults, and iii) a high angle between the younger shortening direction and the axis of the older folds. Some of these factors are present in the NW Persian Gulf. The cover in this area consists of a thick basal layer of evaporites overlain by an alternation of competent-brittle and incompetent-ductile layers (Fig. 1B). Moreover, growth strata coeval with the older deformation accumulated on the limbs but not on the crest of the folds, resulting in a varying load of overburden. Thus, overburden increases from minimum values along the crest of the anticlines to maximum values along the syncline troughs.

Another important factor linked to reactivation is the relation between the Arabian folds and the basement faults. It has been suggested that Arabian folds originate above a basement fault (Edgell, 1991; Alsharhan and Nairn, 1997; Sattarzadeh *et al.*, 2000; Barhroudi and Talbot, 2003). Basement faults, 900 to 600Ma old, are present in the Arabian shield and have been repeatedly reactivated since the late Paleozoic. Thus, it is reasonable to assume that some Arabian trending folds were due to reactivation of basement faults (Edgell, 1996; Abdollahie Fard *et al.*, 2006; Soleimany *et al.*, 2011).

## MODELLING TECHNIQUES

### Analogue materials

The modelling techniques used here are similar to those commonly used for experiments with brittle-ductile systems at the Laboratory of Experimental Tectonics of Géosciences Rennes (Université de Rennes) and have been described in a number of papers (*e.g.* Faugère and Brun, 1984; Vendeville *et al.*, 1987; Davy and Cobbold, 1991). Brittle layers (pre and synkinematic) were represented by dry sand, with an angle of internal friction close to 30° (Krantz, 1991) and a density (ρ) around 1,400kg/$m^3$. Ductile layers were represented by two Newtonian silicone putties (Rhône Poulenc, France). The first one (Silbione: putty "gomme 70009"- Rhône Poulenc, France) is a pink Newtonian material with a viscosity that is temperature dependent (Battegay, 1984). Its viscosity (μ)

is around 2x104Pa·s at 20°C and its density (ρ) is close to 1,200kg/m$^3$. The second silicone putty used (silicone putty "SGM 36"- Rhône Poulenc, France) is a transparent Newtonian material with the viscosity that is also temperature dependent (Weijermars,1986). Its viscosity (μ) is around 3x104Pa·s at 20°C and its density (ρ) is close to 1,000kg/m$^3$. The geometric and dynamic scaling of these models is given in Table 1. The ratios of length and stress between model and nature have the same order (10-5), and the velocity in the model (2cm/h) is compatible with the velocity observed in nature (0,5cm/y) (Pichot *et al.*, 2009; Pinto *et al.*, 2010).

## Experimental procedure

The model was set in a 40x60cm sandbox, wide enough to achieve a relatively large amount of shortening without border effects. The experimental apparatus consisted of a mobile wall with short lateral walls pushed at a constant rate (Fig. 2A). The base of the mobile walls and the base of the sand-silicone pile are at the same level. Displacement of the mobile wall induces deformation of the sand-silicone pile with the formation of thrust faults and folds. All thrust faults end up being connected to the basal silicone layer and to the mobile wall. The experimental apparatus can generate shortening in different directions. Two deformation events were applied in the model. In the first event, shortening was horizontal and perpendicular to the mobile wall in order to simulate an overall pure compression. In the second event, shortening was horizontal but oblique to the mobile wall producing an oblique compression. The angle between the first and second shortening directions is α. The α angles used in the different experiments range between 0° and 83° (0°, 22.5°, 45°, 67.5°, 83°; Fig. 2A). The sand-silicone pile used in the models imitates the stratigraphy in the NW Persian Gulf (Fig. 1A). The prekinematic materials consist of four brittle-ductile layers (Fig. 2A, B) from bottom to top: i) a lower silicone layer 1cm thick (ρ=1,200kg/m$^3$); ii) a lower black and white sand layer 2cm thick; iii) a middle silicone layer 0.7cm thick (ρ=1,000kg/m$^3$) and iv) a middle black and white sand layer 1.5cm thick.

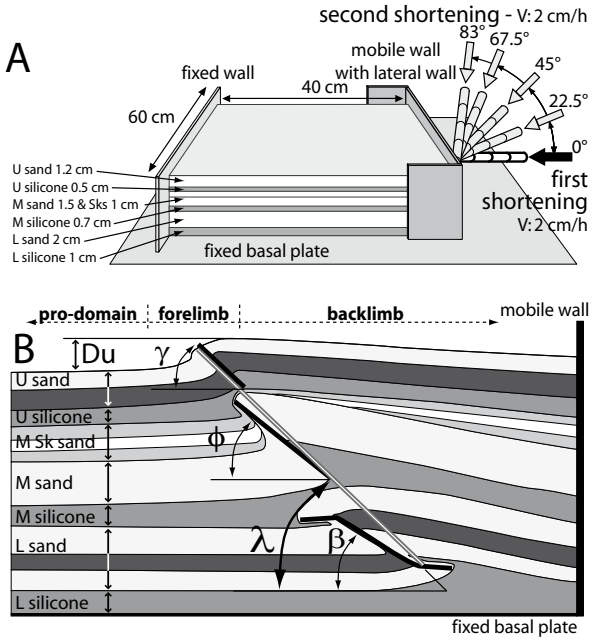


**FIGURE 2** | A) Experimental apparatus showing the angle and velocity of movement of the mobile wall. The model is made up of silicone and sand with lower (L), middle (M) and upper layers (U). In the middle layers, synkinematic sand (Sks) is deposited in the first event of shortening. In all cases, the first and second shortening (arrows) are horizontal but the angle between them changes from one experiment to another. B) Cross-section showing the main deformation features of the model. β, ϕ and γ represent the average dip angles of the thrust faults affecting the lower, middle and upper sands, respectively. λ is the dip angle of the envelope of the thrust faults of the whole structure. ρΔU corresponds to the structural uplift. Further explanations are provided in the text.

In the first event of compression fresh sand was continuously sprinkled manually onto the model during shortening in order to simulate synkinematic sedimentation (Barrier *et al.*, 2002). This sedimentation mode was employed to fill up all the available accomodation space generated by structural uplift. This middle synkinematic layer consisted of blue and white sand with a variable thickness.

After the first deformation event, and before the second one, two layers were deposited on top of the model: the first layer consisted of 0.5cm of silicone (ρ=1,000kg/m$^3$), and the second layer was composed of 1.2cm of black and white sand. These layers were postkinematic with respect to the first deformation event, and prekinematic with respect to the second deformation event. No synkinematic layer with respect to the second deformation event was incorporated into the models. In all the models, a layer of sand was deposited at the end of the experiment to cover the deformed model in order to preserve it for subsequent manipulation.

Photographs of the model surface after the two deformation events show the strike of structures and their arrangement in map-view. Internal structure after deformation was observed in a series of cross-sections cut perpendicular to the mobile wall. Brittle sand layers were built with sand of different colours to reveal structures in the photographs, but these colours did not alter sand behaviour.

Five experiments with only one deformation event and 2cm of shortening were performed in order to select the suitable shortening rate and test the effect of the synkinematic beds. These experiments enabled us to obtain a reproducible geometry at the end of the first event of compression, and to select a velocity of displacement for the mobile wall. The selected velocity was that of 2cm/h.

**TABLE 2** | Results from models after two deformation events. α, angle between the shortening axis of the first and second deformation events. TD2, second deformation event shortening. TD2*, component of the second deformation event shortening parallel to the first deformation event shortening. ΔU, structural uplift (see Fig. 2B). β, φ and γ dip of thrusts faults across lower, middle and upper sand layers, respectively (see Fig. 2B). λ, dip of the envelope of the thrust faults (see Fig. 2B). θ angle between the "en echelon" anticlines and the strike of the thrust fault affecting the middle sand layers (see Fig. 3I, J)

| α | TD2 (cm) | TD2* (cm) | ΔU (cm) | β ± 1 | φ ± 2 | γ ± 2 | λ ± 1 | θ |
|---|---|---|---|---|---|---|---|---|
| 0° | 2 | 2 | 1.52 | 27° | 29° | 15° | 41° | 0° |
| 22.5° | 2 | 1.84 | 1.33 | 28° | 31° | 20° | 42° | 0° |
| 45° | 2 | 1.41 | 1.21 | 29° | 38° | 26° | 44° | 0° |
| 67.5° | 3 | 1.15 | 1 | 30° | 40° | 29/90° | 43° | 0° |
| 83° | 3 | 0.36 | 0.46 | 32° | 38° | /90° | (45°) | 26° |

## RESULTS

The main features of the experiments will be described first. Variability of the observed structures in relation to the angle of compression will be discussed later.

The general shape of the structure is a fold facing the static wall with internal thrust faults and detachment faults branching into a fish-tail structure (Fig. 2B). A fish-tail structure corresponds to conjugate thrusts with opposing vergences generated during horizontal shortening and favoured by the presence of detachment levels (*e.g.* Drozdzewski, 1979; Harrison and Bally, 1988). The top of the upper sand layer shows three domains: i) a pro-domain (in front of the fold close to the fixed wall) where the layers are horizontal; ii) a short forelimb usually affected by a thrust fault and dipping to the fixed wall; and iii) a long backlimb gently dipping towards the mobile wall. Silicone layers (lower, middle and upper) acted as incipient detachment levels. Because of the high velocity of displacement of the mobile wall, each competent layer did not behave independently of each other with the result that the whole pile deformed jointly. This also arises in comparable experiments of compression with several detachment levels where there is only incipient detachment for a velocity higher than 1cm/h, and complete detachment for a velocity lower than 1cm/h (Pichot and Nalpas, 2009). Folds and thrust faults affecting each competent layer have specific geometric characteristics. Thrust faults and folds are characterized by their dip and strike, respectively. β is the dip of the thrust fault cutting the lower sand layer, φ is the dip of the thrust fault cutting the middle sand layers, and γ is the dip of the fault (thrust or strike-slip) cutting the upper sand layer (Fig. 2B). In general β is smaller than φ, which is larger than γ except where this last fault is a strike-slip fault (Table 2). Each thrust fault is located frontward (towards the pro-domain) of the lower one (Fig. 2B). λ is the dip of the envelope of the thrust faults (Fig. 2B). The envelope is the virtual plane connecting the lowermost interruption line in the hangingwall with the uppermost interruption line in the footwall. The crest of the fold generated during the first shortening event is parallel or subparallel to the mobile wall. The structural uplift (ΔU) is the vertical distance between the crest of the fold, created during the second shortening event, and the corresponding horizontal layers in the pro-domain (Fig. 2B).

Figure 3 provides sections of the models from five experiments and surface views of two experiments at the end of the first and second deformation events. Shortening (TD2 in Table 2) was 2cm during the second event in the three first experiments for α equal to 0°, 22.5° and 45° (Fig. 3 A, B, C, G, H) and 3cm in the two last experiments for α equal to 67.5° and 83° (Fig. 3 D, E, F, I, J). The projection of the second shortening normal to the axis of the first shortening (TD2* in Table 2) decreases as α increases (TD2*=cos(α)xTD2). The increase in TD2 is applied to minimise TD2* reduction. The values of the dip of the thrust faults (β, φ, γ and λ) and the structural uplift (ΔU) measured from the cross-sections of the models are given in Table 2. The evolution of the most significant parameters is presented in Figure 4. The structural uplift decreases progressively with the increase in α and the corresponding reduction in the component of the second shortening normal to the fold axis (Table 2, TD2*). Moreover, the aspect of the fish-tail is more apparent for low α angle, showing a larger penetration of sand wedge in the middle silicone layer (Fig. 3). The thrust fault dip is measured with an accuracy of +/-1 degree for β and λ and +/-2 degrees for φ and λ (Table 2). The dip of all the thrust faults increases as α increases. The angle b ranges from 27° to 32° (5 degrees of variation), φ from 29° to 38° (9 degrees of variation) and γ from 15° to 29° (14 degrees of variation). Thus, the range of the dip of the lower thrust fault (β) is smaller than that of the upper thrust fault (γ). The dip of the upper thrust fault is smaller than dip of the lower ones (γ<φ and β) in all the models. Moreover, as α increases, the difference in dip between the lower and upper thrust faults diminishes (from 27° to 15° in the model where α=0°, from 30° to 29° in the model where α=67.5°). As α increases, the dip of the thrust fault envelope (Table 2, angle λ) increases very slowly from 41° to 43° or 45°. This last value is not

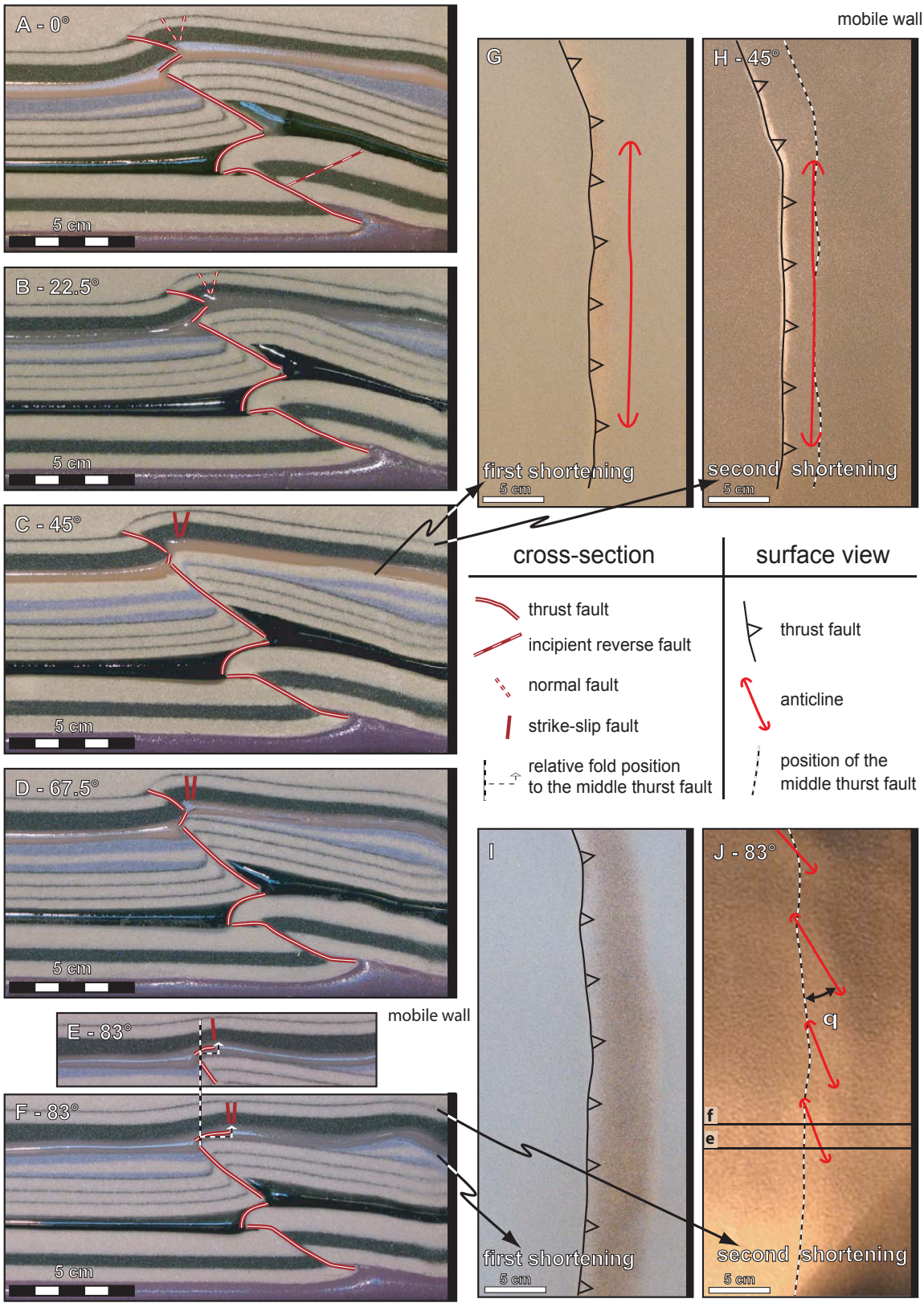


**FIGURE 3** | A), B), C), D) Cross sections of models α=0°, 22.5°, 45° and 67.5°, respectively. E, F) Parallel cross sections of the model with α=83°. G) Surface view after the first shortening event, and H) after the second shortening event for the model with α=45°. I) Surface view after the first shortening event, and J) After the second shortening event for the model with α=83. Location of the cross sections F and E is in J surface view. In the cross sections and surface views the mobile wall is located on the right.

strictly comparable to the others because the upper sand layer is not affected by a thrust fault in this case.

The resulting structure depends on α. In models with low α values (Fig. 3A, B; 0° and 22.5°) a low angle thrust fault affects the upper sand layer with its associated ramp anticline. In addition, normal faults were developed on the crest of this anticline and were slightly rotated during fold evolution in the direction of the pro-domain (especially for α=0°, *e.g.* Emami *et al.*, 2010 or Vergés *et al.*, 2011). In the models with a medium α value (Fig. 3C, D; 45° and 67.5°), after the second shortening, the lower layer is not as folded as in the previous experiments with low α values. The middle layer is affected by a thrust fault but shows a flat backlimb and the upper layer is folded. Normal faults are replaced by strike-slip faults with a normal component on the crest of this anticline. In models with a high α (Fig. 3E, F; 83°), the thrust fault of the upper sand layer is replaced by a strike slip fault. When the models with α values ranging from 0° to 67.5° (Fig. 3A, B, C, D), are observed in surface view (Fig. 3G, H), it may be observed that the thrust fault of the upper sand layer and the anticline crest are parallel to each other. The strike of the anticline and of the lower, middle and upper sand layer thrust faults is the same. This strike is parallel to the mobile wall, and is therefore perpendicular to the first direction of shortening. In the model with an α value of 83° (Fig. 3E, F), the upper sand layer is affected by strike-slip faults and associated folds instead of a thrust fault and a ramp anticline. These folds are arranged in a right-stepping "en echelon" system and their crests are oblique to the mobile wall. The angle between the trend of the "en echelon" folds and the strike of the middle thrust fault is θ (Fig. 3J; Table 2, *e.g.* Richard *et al.*, 1989). In this case, the folds developed above the middle thrust fault in a more backlimb position in relation to the models with a lower α, as observed in the cross-sections (compare Fig. 3E, F and A, B, C, D) or surface views (compare Fig. 3H and J).

## DISCUSSION

Faults generated in the first deformation event acted as weak zones and were reactivated, controlling the localization of the subsequent structures in the second deformation event. In the first deformation event, the synkinematic sedimentation increased the thickness of the brittle layer in the pro-domain and in the backlimb. This induced a lateral variation of the brittle strength: the strength was minimum in the fold crest and in the faulted zone and increased with distance from the fold crest (Pichot and Nalpas, 2009). This weak zone facilitated reactivation of earlier faults as pure dip slip thrust faults or as oblique thrust faults.

Structural style is related to the angle between the two directions of shortening (α). In models of low α (0º to 22.5º), all sand layers show well developed ramp anticlines (Fig. 3A, B) and the thrust faults have a low dip angle that increases slowly with α (Table 2, β, ϕ, λ). In the models of transition between low to medium α (22.5º to 45º), the lower and upper sand layers also display well developed ramp anticlines whereas the medium sand layer shows a regular back tilted hangingwall without a fold (Fig. 3B, C). The dip of the thrust faults displays a large increase (6º-7º) for middle and upper thrust faults, whereas this increase is not significant for the lower thrust fault (Table 2, β, ϕ, λ). This change in the geometry of the structures is attributed to the increase in α and not to the decrease in shortening, which is small in this interval of α (TD2* diminishes from 1.84 to 1.41cm) (Table 2; Fig. 4). In models of medium α (45º to 67.5°) the evolution of the geometry of the structures is similar in the two experiments with a decrease in the uplift (DU) that is less important than the decrease in the shortening (TD2*). In the model of high α (83º), the lower and medium sand layers show a regular back tilted hangingwall and the upper sand layer shows "en echelon" folds and strike-slip faults just above the thrust fault, affecting the medium sand layer (Fig. 3E, F). The trend of the "en echelon" folds forms an angle (θ) of 26º with the strike of the middle thrust fault (Fig. 3E, F, J; Table 2). No significant dip variations of the lower and middle thrust faults are observed when comparison is made with the models of medium α.

The location of structures generated in the second event of shortening is controlled by α. For α ranging from 0º to 67.5º, thrust faults affecting the upper sand layer are systematically located frontward (towards the pro-domain) in relation to the middle thrust fault whereas for α=83º the "en echelon" folds and strike-slip faults are located in a backward position (Fig. 3E).

The evolution of the uplift (DU) compared with the normal shortening (TD2*) is not linear (Fig. 4). For low α (0º to 22.5º), the evolution corresponds to a compressive regime, but for the transition to medium α (22.5º to 45º), the uplift decreases less than the shortening owing to strain partitioning, and for high α (83°), the decrease of the uplift is considerable due to the strike-slip regime.

Our experiments are consistent with earlier results of analogue modelling of compressive and transpressive systems, where the increase in the thrust dip is favoured by synkinematic sedimentation (Barrier *et al.*, 2002; Pichot and Nalpas, 2009, Casas *et al.*, 2001). Moreover, the increase in thrust dip after the second shortening event is also favoured by the increase in the strike-slip movement (Casas *et al.*, 2001). A variation of strain context from compressive to strike-slip was also confirmed by this study.

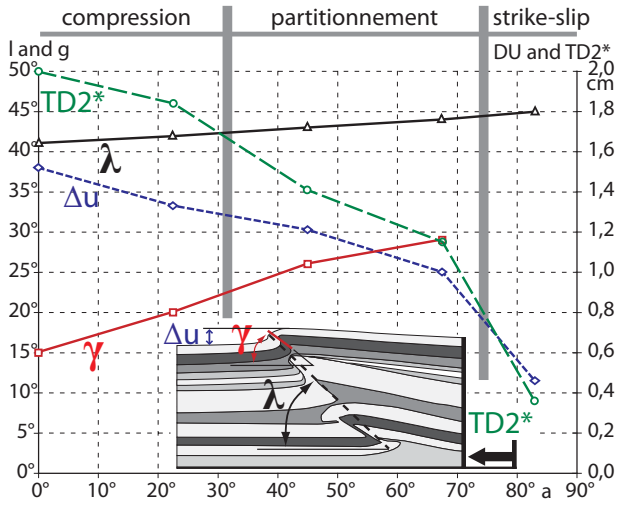


**FIGURE 4** | Graph showing the evolution of the thrusts dip angle (γ and λ), the structural uplift (ΔU) and the component of the second shortening event parallel to the first shortening event (TD2*) (see Fig. 2B) with respect to the angle of the second shortening direction (α).

## COMPARISON BETWEEN THE MODELS AND THE STRUCTURES IN THE NW PERSIAN GULF

Analogue modelling shows that the structural style is considerably influenced by the angle between the axis of the folds formed in the first deformation and the shortening direction of the second deformation. In the models with a stratigraphic pile comparable to that in the Persian Gulf, the folds formed in the first deformation are reactivated if the angle between their axis and the shortening direction of the second deformation is 90°– 67.5°=22.5° or larger. If this angle is 90°- 83°=7° or smaller, *i.e.* that is if the axis of the folds formed in the first deformation and the shortening direction of the second deformation are parallel or almost parallel, fold reactivation does not occur. In this case, a set of "en echelon" folds and strike slip faults develop in the upper brittle layers. In the NW Persian Gulf, the angle between the Arabian trend (N024E) and the Zagros shortening (perpendicular to the Zagros trend - N125E) is around 10° as deduced from Figure 1E. Thus, angular relations between the Arabian fold trend and the Zagros shortening are at the limit for fold reactivation with the result that reactivation can be facilitated by additional factors (anticlines A1 M, A3 M and north trending part of A8 M, Fig. 1E) whereas in less favourable cases, in addition to reactivated folds, a fold interference pattern is produced (anticlines A2 M, A5 M and A8 M, Fig. 1E).

In the models, structures resulting from the second deformation were controlled by structures generated during the first deformation and by the thickness distribution of synkinematic sediments. In the NW Persian Gulf, seismic sections (*e.g.* Fig. 1C) show that older folds played an important role in the younger shortening event. In some cases, the longitudinal strength of the Arabian trending folds was enough to prevent the formation of a dome-basin fold interference pattern. On the other hand, the crest of the Arabian folds acted as a weak zone where deformation was concentrated. This weak zone resulted from the thin overburden due to the absence of Late Cretaceous synkinematic sediments. It is not surprising that in some cases the effect of the younger shortening was to reactivate the Arabian trending folds by tightening them.

In the models "en echelon" folds are generated when the shortening direction is close to the strike of the earlier structures. This suggests that this type of fold could be produced during reactivation of the Arabian trending folds given the proximity of the Zagros shortening direction to the trend of the Arabian folds. In such a case, the Arabian trending folds could depart from a simple cylindrical geometry and could be disrupted by minor anticlines and saddles arranged "en echelon". This is crucial to the oil industry because these second order "en echelon folds" would affect considerably the volume and geometry of the main anticline closure. Currently, these folds cannot be detected with the available seismic survey data because of the distance between adjacent seismic lines.

Finally, in the experiments performed no basement structures (neither folds nor faults) were modelled below the lower silicone layer. Thus, the models presented in this paper show that, with a favourable stratigraphic pile such as the one used in our models, basement faults are not necessary for the reactivation of compressive structures that are subsequently shortened at variable angles to their trend. Nevertheless, basement faults can contribute to reactivation and should not be excluded. As stated above, basement faults could be responsible for some Late Cretaceous Arabian folds. Moreover, Soleimany *et al.* (2011) conclude that halokinesis of salt from the lower ductile layer plays a major role in the reactivation of the Dorood anticline, which is a Late Cretaceous Arabian fold, and suggest that halokinesis could be controlled by the reactivation of an old basement fault.

## CONCLUSIONS

Folds and faults that developed in the models during the first event of shortening create a weak zone. The synkinematic sediments increase in thickness and strength with distance from the folded and faulted zone. Hence, during the second deformation, it is easier to reactivate earlier faults that lead to fold reactivation rather than generation of new faults.

Structural style in the models resulting from the two deformations is related to the angle (α) between the two directions of shortening. The earlier faults are reactivated in the second event of shortening: i) as almost pure thrust faults for low α values; ii) as oblique thrust faults for medium α values

with strain partitioning; and iii) as strike-slip thrust faults with a higher strike-slip component for high α values. The upper thrust faults are associated with ramp anticline and located frontward (towards the pro-domain) of the lower thrust fault for low and medium α values, whereas "en echelon" folds and strike-slip faults are developed upward (*i.e.* in the backlimb above the underlying thrust) for high α values.

Obviously the folds in the models are not exact reproductions of the Arabian folds in the NW Persian Gulf. Nevertheless, these models are helpful in understanding some of the features of the Arabian folds. Three points should be noted: i) the stratigraphy of the NW Persian Gulf is well suited to the late Cenozoic reactivation of the Late Cretaceous Arabian folds because of the thick ductile layer in the lower part of the cover, the alternating competent-incompetent layers and the reduction in the overburden load towards the anticline crest; ii) the Zagros shortening and the Arabian trend are not parallel, although the angle between these two directions is small, it is large enough to permit reactivation of some Arabian folds in the late Cenozoic; and iii) no strike-slip faults and "en echelon" folds affecting the cover and associated with the Arabian folds are observed in the NW Persian Gulf. By contrast, a fold interference consisting of an S-shaped trend is produced in the cases of the Arabian folds that are not suitably oriented for reactivation. This observation indicates that reactivation is critical, *i.e.* that is, small variations in the direction of Zagros shortening, in the trend of the Arabian folds or in the mechanical stratigraphy could either prevent or enhance reactivation. It should be noted that the value of the angle between the Zagros shortening and the Arabian trend plays a crucial role. Reactivation would be much more difficult or impossible if it were smaller.

## ACKNOWLEDGMENTS

The authors are indebted to the Exploration Directorate of the National Iranian Oil Company (NIOC) for providing all the data required for this study. Thanks are also due to M. Mohaddes, M. Zadehmohammadi, S. Javadian, R. Nematollahi, D. Baghbani, M.M. Khorasani, M.A. Naini, I. Abdollahie Fard, G. A. Fakoori, M.G.H. Goodarzi, S. Sherkati, M. Sepehr, M.A. Parham, M. Aliee, M. Rahimi, H. Ramesh, F. Gholami, M. Hajian, N. Pasdar, F. Beik and M. Allahyari .

This work has been partially funded by the following Spanish Research Projects: "Consolider, Topo-Iberia" (CSD2006-00041), "Modelización Estructural 4 D" (CGL2007-66431-C02-01/BTE) and "El Significado del Promontorio Balear" (CGL2008-05724/BTE). We are grateful to Abbas Barhoudi and Emilio Casciello for reviewing the manuscript. We are also indebted to John Cosgrove and Antonio Casas for their helpful comments on an earlier version of this paper and to George von Knorring for reviewing the English.

## REFERENCES

Abdollahie Fard, I., Braathen, A., Mokhtari, M., Alavi, A. 2006. Interaction of the Zagros Fold-Thrust Belt and the Arabian-type, deep-seated folds in the Abadan Plain and the Dezful Embayment, SW Iran. Petroleum Geoscience, 12, 347-362.

Alavi, M., 1994. Tectonics of the Zagros orogenic belt of Iran: new data and interpretations. Tectonophysics, 229, 211-238.

Allemand, P., Brun, J.-P., Davy, P., Van Den Driessche, J., 1989. Symétrie et asymétrie des rifts et mécanismes d'amincissement de la lithosphère. Bulletin de la Société Géologique de France, 3(V), 445-451.

Alsharhan, A.S., Nairn, A.E.M., 1997. Sedimentary Basins and Petroleum Geology of the Middle East. Amsterdam, Elsevier Science, 280pp.

Bahroudi, A., Talbot, C.J., 2003. The configuration of the basement beneath the Zagros Basin. Journal of Petroleum Geology, 26(3), 257-282.

Balé, P., 1986. Tectonique cadomienne en Bretagne nord. Interaction décrochement chevauchement: champs de déformation et modélisations expérimentales. Thèse de 3ème cycle. Université de Rennes 1, 361pp.

Ballard, J.F., 1989. Approche géologique et mécanique des décollements dans la croûte supérieure. Thèse de Doctorat. Université de Rennes 1, 301pp.

Barrier, L., Nalpas, T., Gapais, D., Proust, J.-N., Casas, A., Bourquin, S., 2002. Influence of syntectonic sedimentation on thrusts geometry. Field examples from the Iberian Chain (Spain) and analogue modeling. Sedimentary Geology, 146, 91-104.

Beydoun, Z.R., 1991. Arabian plate hydrocarbon geology and potential - a plate tectonic approach. American Association of Petroleum Geologists Studies in Geology, 33.

Brun, J.P., Nalpas, T., 1996. Graben inversion in nature and experiments. Tectonics, 15(2), 677-687.

Casas, A.M., Gapais, D., Nalpas, T., Besnard, K., Roman Berdiel, T., 2001. Analogue models of transpressive systems. Journal of Structural Geology, 23(5), 733-743.

Casciello, E., Vergés, J., Saura, E., Casini, G., Fernández, N., Blanc, E., Homke, S., Hunt, D.W., 2009. Fold patterns and multilayer rheology of the Lurestan Province, Zagros Simply Folded Belt (Iran). London, Journal of the Geological Society, 166, 947-959. DOI:10.1144/0016-76492008-138

Davy, P., Cobbold, P.R., 1991. Experiments on shortening of a 4-layer model of continental lithosphere. Tectonophysics, 188, 1-25.

Dewey, J.F., Holdswoth, R.E., Strachan, R.A. 1998. Transpression and transtension zones. London, Geological Society, 135 (Special Publications), 1-14.

Drozdzewski, G., 1979. Grundmuster der Falten – und Bruchstrukturenim Ruhrkarbon. Zeitschrift deutsche. Geologische Gesellscharft, 130, 51-67.

Dubois, A., Odonne, F., Massonnat, G., Lebourg, T., Fabre, R., 2002. Analogue modeling of fault reactivation: tectonic inversion and oblique remobilisation of grabens. Journal Structural Geology, 24, 1741-1752.

Edgell, H.S., 1991. Proterozoic salt basins of the Persian Gulf area and their role in hydrocarbon generation. Precambrian Research, 54, 1-4.

Edgell, H.S., 1996. Salt tectonism in the Persian Gulf Basin. In: Alsop, G.L., Blundell, D.J., Davison, I. (eds.). Salt Tectonics. London, Geological Society, 100 (Special Publications), 129-151.

Emami, H., Vergés, J., Nalpas, T., Gillespie, P., Sharp, J., Karpuz, R., Blanc, E.P., Goodarzi, M.G.H., 2010. Structure of the Mountain Front Flexure along the Anaran Anticline in the Pusht-E-Kuh Arc (NW Zagros, Iran): insights from sand box models. In: Leturmy, P., Robin, C. (eds.). Tectonic and Stratigraphic Evolution of Zagros and Makran during the Mesozoic–Cenozoic. London, Geological Society, 330 (Special Publications), 155-178. DOI: 10.1144/SP330.9 0305-8719/10/

Faccenna, C., Nalpas, T., Brun, J.P., Davy, P., 1995. The influence of preexisting thrust faults on normal fault geometry in nature and in experiments. Journal of Structural Geology, 17, 1139-1149.

Faugère, E., Brun, J.P., 1984. Modélisation expérimentale de la distension continentale. Comptes Rendus de l'Académie des Sciences, Série II, 299, 365-370.

Gestain, V., Nalpas, T., Rouby, D., Barrier, L., 2004. Rôle des niveaux incompétents syncinématiques sur l'évolution des structures chevauchantes. Bulletin de la Société Géologique de France, 175(4), 351-359.

Harding, T.P., 1985. Seismic characteristics and identification of negative flower structures, positive flower structures and positive structural inversion. American Association Petroleum Geology Bulletin, 69, 582-600.

Harrison, J.C., Bally, A.W., 1988. Cross sections of the Parry Islands fold belt on Melville Island. Canadian Petroleum Geology Bulletin, 36, 311-332.

Homke, S., Vergés, J., Garcés, M., Emami, H., Karpuz, R., 2004. Magnetostratigraphy of Miocenen-Pliocene Zagros foreland deposits in the front of the Push-e Kush Arc (Lurestan Province, Iran). Earth and Planetary Science Letters, 225, 397-410.

James, G.A., Wynd, J.G., 1965. Stratigraphic nomenclature of Iranian Oil Consortium Agreement Area. American Association Petroleum Geology Bulletin, 49, 2182-2245.

Krantz, R.W., 1991. Measurements of friction coefficients and cohesion for faulting and fault reactivation in laboratory models using sand and sand mixtures. Tectonophysics, 188, 203-207.

Koopman, A., Speksnijder, A., Horsfield, W.T., 1987. Sandbox model studies of inversion tectonics. Tectonophysics, 137, 379-388.

Letouzey, J., 1990. Fault reactivation, inversion and fold-thrust belt. In: Letouzey, J. (ed.). Petroleum and tectonic in Mobile belts. Paris, Technip, 101-128.

Malavielle, J., 1984. Modélisation expérimentale des chevauchements imbriqués: application aux chaînes de montagnes. Bulletin de la Société Géologique de France, XXVI(1), 129-138.

Mescua, J.F., Giambiagi, L.B., 2012. Fault inversion vs. new thrust generation: A case study in the Malargüe fold-and-thrust belt, Andes of Argentina. Journal of Structural Geology, 35, 51-63. DOI: 10.1016/j.jsg.2011.11.011

Nalpas, T., le Douaran, S., Brun, J.P., Unternehr, P., Richert, J.P., 1995. Inversion of the Broad Fourteens Basin (offshore Netherlands), a small-scale model investigation. Sedimentary Geology, 95, 237-250.

Nalpas, T., Gapais, D., Vergés, J., Barrier, L., Gestain, G., Leroux, G., Rouby, D., Kermarrec, J.J., 2003. Effects of rate and nature of synkinematic sedimentation on the growth of compressive structures constrained by analogue models and field examples. Geological Society of London, 208 (Special Publications), 307-319.

O'Brien, C.A.E., 1950. Tectonic problems of the oilfield belt of the soutwest Iran. In: Buiter, J. (ed.). 18th International Geological Congress. Great Britain, Proceedings, 6, 45-58.

Pinto, L., Muñoz, C., Nalpas, T., Charrier, R., 2010. Role of sedimentation during basin inversion in analogue modelling. Journal Structural Geology, 32(4), 554-565. DOI: 10.1016/j.jsg.2010.03.001

Pichot, T., Nalpas, T., 2009. Influence of synkinematic sedimentation in a thrust system with two decollement levels; analogue modelling. Tectonophysics, 473, 466-475. DOI: 10.1016/j.tecto.2009.04.003

Ramsay, J.G., Huber, M.I., 1987. The techniques of Modern Structural Geology. Volume 2: Folds and Fractures. London, Academic Press, 700pp.

Richard, P., Ballard, J.F., Colletta, B., Cobbold, P., 1989. Naissance et évolution de failles au dessus d'un décrochement de socle: Modélisation analogique et tomographie. Comptes Rendus de l'Académie des Sciences de Paris, Série IIa, 309, 2 111-2 118.

Richard, P., Cobbold, P., 1990. Experimental insights into partioning fault motions in continental convergent wrench zones. Annales Tectonicae, 4, 35-44.

Richard, P., Krantz., 1991. Experiments on fault reactivation in strike-slip mode. Tectonophysics, 188, 117-131.

Richard, P., Mocquet, B., Cobbold, P., 1991. Experiments on simultaneous faulting and folding above a basement wrench fault. Tectonophysics, 188, 133-141.

Sassi, W., Colletta, B., Balé, P., Paquereau, T., 1993. Modelling of structural complexity in sedimentary basins: the role of pre-existing faults in thrust tectonics. Tectonophysics, 226, 97-112.

Sattarzadeh, Y., Cosgrove, J.W., Vita Finzi, C., 2000. The interplay of faulting and folding during the evolution of the Zagros deformation belt. In: Cosgrove, J.W., Ameen, M.S. (eds.). Forced folds and fractures. London, Geological Society, 169 (Special Publications), 187-196.

Saura, E., Vergés, J., Homke, S., Blanc, E., Serra-Kiel, J., Bernaola, G., Casciello, E., Fernández, N., Romaire, I., Casini, G. Embry, J.Ch., Sharp, I.R., Hunt, D., 2011. Basin architecture and growth folding of the NW Zagros early foreland basin during the Late Cretaceous and early Tertiary. London, Journal of the Geological Society, 168, 235-250.

Sella, G.F., Dixon, T.H., Mao, A.L., 2002. REVEL: A model for recent plate velocities from space geodesy. Journal of Geophysical Research – Solid Earth, 107, B4, 2081. DOI:10.1029/2000JB000033

Sepehr, M., Cosgrove, J.W., Moieni, M., 2006. The impact of cover rock rheology on the style of folding in the Zagros fold-thrust Belt. Tectonophysics, 427, 265-281.

Sibson, R.H., 1985. A note on fault reactivation. Journal of Structural Geology, 7, 751-754.

Soleimany, B., Sàbat, F., 2010. Style and age of deformation in the Northwest Persian Gulf. Petroleum Geosciences, 15, 1-10. DOI: 10.1144/1354-079309-837

Soleimany, B., Poblet, J., Bulnes, M., Sàbat, F., 2011. Fold amplification history unravelled from growth strata: the Dorood anticline, NW Persian Gulf. London, Journal of Geological Society, 168, 219-234. Doi: 10.1144/0016-76492010-085

Stern, R.J., 1985. The Najd fault system, Saudi Arabia and Egypt: a late Precambrian rift-related transform system. Tectonics, 4, 497-511.

Stöcklin, J., 1968. Structural History and Tectonics of Iran: a review. American Association Petroleum Geology Bulletin, 52(7), 1229-1258.

Vendeville, B., Cobbold, P., Davy, P., Brun, J.P., Choukroune, P., 1987. Physical models of extensional tectonics at various scales. In: Coward, J.F., Dewey, J.F., Hancock, P.L. (eds.). Continental extensional tectonics. Geological Society of London, 28 (Special Publications), 95-107.

Vergés, J., Goodarzi, M.H., Emami, H., Karpuz, R., Efstathiou, J., Guillespie, P., 2009. Multiple detachment folding in Pusht-e Kuh arc, Zagros: Role of mechanical stratigraphy. In: McClay, K., Shaw, J., Suppe, J. (eds.). Thrust Fault-related Folding. American Association of Petroleum Geologists, 94 (Memoirs), 1-26.

Vergés, J., Saura, E., Casciello, E., Fernàndez, M., Villaseñor, A., Jiménez-Munt, I., García-Castellanos, D., 2011.Crustal-scale cross-sections across the NW Zagros belt: implications for the Arabian margin reconstruction. Geological Magazine, 148(5-6), 739-761.

Weijermars, R., 1986. Flow behaviour and physical chemistry of bouncing putties and related polymers in view of tectonic laboratory applications. Tectonophysics, 124, 325-358.

**Manuscript received May 2012;**
**revision accepted January 2013;**
**published Online April 2013.**